Journal of Sound and Vibration 329 (2010) 1126–1136

Contents lists available at ScienceDirect

Journal of Sound and Vibration

journal homepage: www.elsevier.com/locate/jsvi

Free vibration analysis of piezoelectric coupled circular plate with open circuit

N. Wu [a], Q. Wang [a,*], S.T. Quek [b]

[a] Department of Mechanical and Manufacturing Engineering, University of Manitoba, Winnipeg, Manitoba, Canada R3T 5V6
[b] Department of Civil Engineering, National University of Singapore, 117576 Singapore

ARTICLE INFO

Article history:
Received 25 March 2009
Received in revised form
11 September 2009
Accepted 29 October 2009
Handling Editor: A.V. Metrikine
Available online 24 November 2009

ABSTRACT

A vibration analysis of a circular steel substrate surface bonded by a piezoelectric layer with open circuit is presented. A solution for the electrical potential along the thickness direction of the piezoelectric layer satisfying the open circuit electric boundary condition is developed for the first time. The mechanical model and solutions for the vibration analysis of the piezoelectric coupled circular plate are then established based on the developed electrical potential, the Kirchhoff plate model, and the Maxwell equation. The first four mode shapes and the corresponding resonant frequencies of the plate with two standard boundary conditions are presented in numerical simulations and compared with those of a piezoelectric coupled plate with the closed circuit condition. The simulations show that the resonant frequencies of the open circuit piezoelectric coupled plate are higher than those of the closed circuit piezoelectric coupled plate. Corresponding discussions are thus provided for the higher piezoelectric effect from the open circuit piezoelectric layer.

1. Introduction

A metal substrate surface bonded or embedded by a piezoelectric layer has been intensely studied during last two decades for practical designs of actuators, sensors, and absorbers because of the electromechanically coupling characteristics. Examples include the actuation analysis of piezoelectric fiber composites [1], vibration, and buckling of piezoelectric coupled laminated structures [2,3], and wave propagation in piezoelectric coupled cylinder structures [4]. The analyses about the structural vibration and control were also conducted with different piezoelectric coupled structures [5–9].

Fundamental mechanical models for analysis of piezoelectric coupled structures are indispensable and have been attracted much attention. Crawley and deLius [10] developed a uniform strain model for a beam with surface bonded and embedded piezoelectric actuator patches accounting for the shear lag effects of the adhesive layer between the piezoelectric actuator and the host beam. A model to account for the coupling effect was later proposed based on the Euler beam assumption [11]. Based on Hamilton's principle, Leibowitz and Vinson [12] derived a model in which the elastic layers, soft-core layers or piezoelectric layers are included. A meshfree model was constructed by Liew et al. [13] for the static analysis of laminated composite beams and plates with integrated piezoelectric layer based on the element-free Galerkin (EFG) method.

* Corresponding author. Tel.: +1 204 474 6443.
E-mail address: q_wang@umanitoba.ca (Q. Wang).

0022-460X/$ - see front matter © 2009 Elsevier Ltd. All rights reserved.
doi:10.1016/j.jsv.2009.10.040

Piezoelectric materials with both closed and open circuit boundary conditions are widely applied in engineering applications. For example, the closed circuit piezoelectric materials are mostly used for the design of ultrasonic motors and resonators, and the open circuit piezoelectric materials are employed for the design of vibration sensors and absorbers. Wang and Quek [14] presented a study of a free vibration of a piezoelectric sandwich beam structure, in which the piezoelectric effect on resonance frequencies of the structure and the distribution of the electric potential were investigated and analyzed. In addition, a quadratic electrical distribution in thickness direction of the piezoelectric layer was proposed by Wang et al. [15] in analysis of a piezoelectric coupled circular plate with closed circuit condition. In analysis of the open circuit piezoelectric materials, Davis and Lesieutre [16] studied a vibration absorber using a piezoelectric material, and found the effective stiffness of the piezoelectric material would increase when the electric surface condition changes from closed to open circuit. Corr and Clark [17] employed the high stiffness of the structure induced by the open circuit piezoelectric material to increase the structure damping and potential energy. Chevallier and Ghorbel [18] experimentally presented a benchmark for free vibration and effective coupling of thick piezoelectric smart structures. Liu, Pan, Heyliger, and Ding [19–22] studied the free vibration process of piezoelectrically coupled plate with both open and closed circuit electric surface conditions. Their research showed that the coupled plate vibration response with open circuit piezoelectric layer is far different from the one with closed circuit piezoelectric layer. From the authors' knowledge, most of the available researches studied the open circuit piezoelectric coupled plates through finite element method (FEM) simulations and experimental investigations. An accurate physical model of the piezoelectric coupled plate with open circuit electric boundary condition, especially the electrical potential distribution along the thickness direction of the piezoelectric layer, needs to be developed.

The free vibration analysis of a thin piezoelectric coupled circular plate with open circuit electric surface condition is presented. A solution for the electrical potential across piezoelectric layers' thickness is developed the first time to strictly satisfy the open circuit electrical boundary condition. Based on the derived electric potential, the Kirchhoff plate model, and the Maxwell equation, a mechanical model for the open circuit piezoelectric coupled circular plate is established. System resonance frequencies and displacement mode shapes are provided by numerical simulations. Moreover, the resonant frequencies of the plate are compared with the results of closed circuit condition [15], and an attempt on physical interpretation of the difference of the resonant results is included. The potential application of this research lies in the design of piezoelectric sensors and absorbers and structural vibration control using piezoelectric materials.

2. Mechanical models for piezoelectrically coupled circular plate with open circuit condition

In the following vibration analysis of the cylinder plate, the cylindrical coordinate system is adopted. z-Axis indicates the thickness direction.

2.1. Kinematics and constitutive relations

In this section, basic kinematics and constitutive equations of the piezoelectric layer and the host plate are simply provided for derivations of the free vibration of the coupled plate in later sections. The structure of a piezoelectric coupled circular plate with radius r_0 is shown in Fig. 1. The thickness of piezoelectric layer and the half thickness of the host plate are denoted as h_1 and h. In application of the Kirchhoff thin plate theory, the displacements and strains of the plate are provided:

$$u_z = u_z(r,\ \theta,\ t) = w(r,\ \theta,\ t) \tag{1}$$

$$u_r = u_r(r,\ \theta,\ t) = -z\frac{\partial u_z}{\partial r} \tag{2}$$

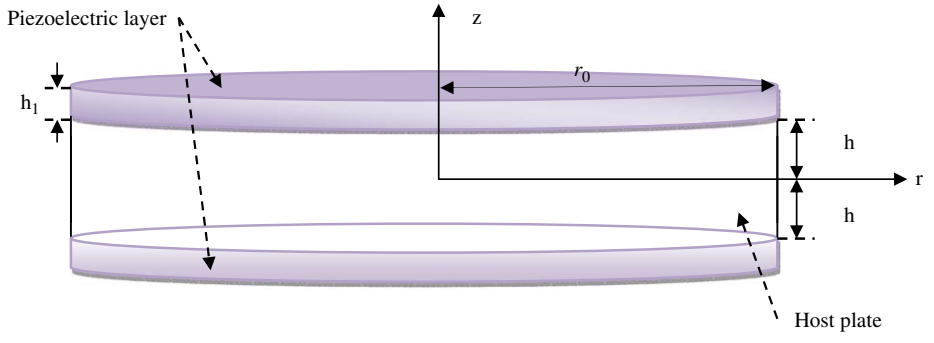

Fig. 1. Layout of a circular plate with two piezoelectric layers mounted on its surfaces.

$$u_\theta = u_\theta(r,\ \theta,\ t) = -z\frac{\partial u_z}{r\partial\theta} \tag{3}$$

$$\varepsilon_{rr} = \frac{\partial u_r}{\partial r} = -z\frac{\partial^2 w}{\partial r^2} \tag{4}$$

$$\varepsilon_{\theta\theta} = \frac{\partial u_\theta}{r\partial\theta} + \frac{u_r}{r} = -z\left(\frac{\partial^2 w}{r^2\partial\theta^2} + \frac{\partial w}{r\partial r}\right) \tag{5}$$

$$\varepsilon_{r\theta} = \frac{1}{2}\left(\frac{\partial u_r}{r\partial\theta} + \frac{\partial u_\theta}{\partial r} - \frac{u_\theta}{r}\right) = -z\left(\frac{\partial^2 w}{r\partial r\partial\theta} - \frac{\partial w}{r^2\partial\theta}\right) \tag{6}$$

where u_z, u_r, and u_θ are the displacements in the transverse z-direction, radial r-direction, and tangential θ-direction of the plate, respectively.

The stress components in the host plate are thus expressed as

$$\sigma^1_{rr} = \frac{E}{1-\mu^2}(\varepsilon_{rr} + \mu\varepsilon_{\theta\theta}) = -\frac{Ez}{1-\mu^2}\left[\frac{\partial^2 w}{\partial r^2} + \mu\left(\frac{\partial^2 w}{r^2\partial\theta^2} + \frac{\partial w}{r\partial r}\right)\right] \tag{7}$$

$$\sigma^1_{\theta\theta} = \frac{E}{1-\mu^2}(\varepsilon_{\theta\theta} + \mu\varepsilon_{rr}) = -\frac{Ez}{1-\mu^2}\left(\frac{\partial^2 w}{r^2\partial\theta^2} + \frac{\partial w}{r\partial r} + \mu\frac{\partial^2 w}{\partial r^2}\right) \tag{8}$$

$$\tau^1_{r\theta} = -\frac{Ez}{1+\mu}\left(\frac{\partial^2 w}{r\partial r\partial\theta} - \frac{\partial w}{r^2\partial\theta}\right) \tag{9}$$

The piezoelectric material is assumed to be polarized in the z-direction. The stress components in piezoelectric layer can be written as

$$\sigma^2_{rr} = \overline{C}^E_{11}\varepsilon_{rr} + \overline{C}^E_{12}\varepsilon_{\theta\theta} - \overline{e}_{31}E_z \tag{10}$$

$$\sigma^2_{\theta\theta} = \overline{C}^E_{12}\varepsilon_{rr} + \overline{C}^E_{11}\varepsilon_{\theta\theta} - \overline{e}_{31}E_z \tag{11}$$

$$\tau^2_{r\theta} = (\overline{C}^E_{11} - \overline{C}^E_{12})\varepsilon_{r\theta} = -z(\overline{C}^E_{11} - \overline{C}^E_{12})\left(\frac{\partial^2 w}{r\partial r\partial\theta} - \frac{\partial w}{r^2\partial\theta}\right) \tag{12}$$

where the superscripts 1 and 2 represent the variables in the host structure and the piezoelectric material, respectively; $\bar{C}^E_{11}$, $\bar{C}^E_{12}$ and $\bar{e}_{31}$ are transformed reduced material constants of piezoelectric medium for plane stress problem, and are given by $\bar{C}^E_{11}=C^E_{11}-((C^E_{13})^2/C^E_{33})$, $\bar{C}^E_{12}=C^E_{12}-((C^E_{13})^2/C^E_{33})$, $\bar{e}_{31}=e_{31}-(C^E_{13}e_{33}/C^E_{33})$ [19]. E is Young's modulus of beam material; C^E_{11} and C^E_{12} are the elastic modulus of piezoelectric material in the radial and tangential directions measured at constant electric field; and e_{31} is the piezoelectric constant of the piezoelectric layer.

2.2. Electric potential distribution in the piezoelectric layer

A quadratic variation of the electric potential in the transverse direction of the closed circuit piezoelectric layer was provided by Wang et al. [15], and verified by the finite element analysis. An electric potential solution for the open circuit piezoelectric layer needs to be established to strictly satisfy the open circuit electrical boundary condition. The potential function in thickness direction of open circuit piezoelectric layer is first assumed to be

$$\phi = \left[1 - \left(\frac{z-h-h_1/2}{h_1/2}\right)^2\right]\varphi(r,\ \theta,\ t) + X, \tag{13}$$

where X is a linear function of z, $X=Az+B$. A and B are parameter functions of r, θ, and t. They will be determined to satisfy the open circuit electric boundary conditions. Since the piezoelectric layer is surface bonded on the metal substrate, the electric potential on the interface of the layer and substrate is null. Meanwhile, since the piezoelectric layer abuts the vacuum, i.e. the surface of the piezoelectric layer is totally isolated and insulated; the electric displacement at the surface can be approximated to be zero [23]. Eq. (13) should satisfy the following boundary conditions

$$\begin{aligned} \phi|_{z=h} &= 0 \\ D_z|_{z=h+h1} &= 0 \end{aligned} \tag{14}$$

where ϕ is the electric potential, and D_z is the corresponding electric displacement along the z-direction.

Submitting Eq. (13) into the three components of the electric field and electric displacement yields

$$E_r = -\frac{\partial \phi}{\partial r} = -\left[1-\left(\frac{z-h-h_1/2}{h_1/2}\right)^2\right]\frac{\partial \varphi}{\partial r} - \frac{\partial X}{\partial r} \tag{15}$$

$$E_\theta = -\frac{\partial \phi}{r\partial \theta} = -\left[1-\left(\frac{z-h-h_1/2}{h_1/2}\right)^2\right]\frac{\partial \varphi}{r\partial \theta} - \frac{\partial X}{r\partial \theta} \tag{16}$$

$$E_z = -\frac{\partial \phi}{\partial z} = \frac{8(z-h-h_1/2)}{h_1^2}\varphi - \frac{\partial X}{\partial z} \tag{17}$$

$$D_r = \overline{\Xi}_{11}E_r = -\overline{\Xi}_{11}\left[1-\left(\frac{z-h-h_1/2}{h_1/2}\right)^2\right]\frac{\partial \varphi}{\partial r} - \overline{\Xi}_{11}\frac{\partial X}{\partial r} \tag{18}$$

$$D_\theta = \overline{\Xi}_{11}E_\theta = -\overline{\Xi}_{11}\left[1-\left(\frac{z-h-h_1/2}{h_1/2}\right)^2\right]\frac{\partial \varphi}{r\partial \theta} - \overline{\Xi}_{11}\frac{\partial X}{r\partial \theta} \tag{19}$$

$$D_z = \overline{\Xi}_{33}E_z + \overline{e}_{31}(\varepsilon_{rr}+\varepsilon_{\theta\theta}) = \overline{\Xi}_{33}\frac{8(z-h-h_1/2)}{h_1^2}\varphi - \overline{\Xi}_{33}\frac{\partial X}{\partial z} + \overline{e}_{31}(\varepsilon_{rr}+\varepsilon_{\theta\theta}) \tag{20}$$

where $\overline{\Xi}_{11}$ and $\overline{\Xi}_{33}$ are reduced dielectric constants of the piezoelectric layer for a plane stress problem, which are given by $\overline{\Xi}_{11}=\Xi_{11}$, $\overline{\Xi}_{33}=\Xi_{33}+(e_{33}^2/C_{33}^E)$, E_r, E_θ, and E_z are the electric field intensity in the r, θ, and z directions, respectively; D_r, D_θ, and D_z are the corresponding electric displacements; Ξ_{11} and Ξ_{33} are the dielectric constants of the piezoelectric layer; Δ is the Laplace operator and is given by $\Delta=(\partial^2/\partial r^2)+(\partial/r\partial r)+(\partial^2/r^2\partial\theta^2)$.

Substitution of Eqs. (13) and (20) into electric boundary conditions given by Eq. (14) leads to the expressions of unknown constants A and B, and the expression of the electric potential in Eq. (13) becomes

$$\phi = \left[1-\left(\frac{z-h-h_1/2}{h_1/2}\right)^2\right]\varphi(r,\ \theta,\ t) + \frac{4(z-h)}{h_1}\varphi(r,\ \theta,\ t) - \frac{\overline{e}_{31}}{\overline{\Xi}_{33}}(h+h_1)(z-h)\Delta w. \tag{21}$$

Eq. (21) is the electric distribution function along the thickness direction of open circuit piezoelectric layer.

2.3. Analysis of piezoelectric coupled circular plate

Substitution of Eqs. (21) and (17) into Eqs. (10)–(12) yields three components of the resultant moments in the coupled plate

$$M_{rr} = \int_{-h-h_1}^{h+h_1} z\sigma_{rr}\,dz = \int_{-h}^{h} z\sigma_{rr}^1\,dz + 2\int_{h}^{h+h_1} z\sigma_{rr}^2\,dz = -\left[(D_1+D_2)\frac{\partial^2 w}{\partial r^2} + \left(\mu D_1 + \frac{\overline{C}_{12}^E}{\overline{C}_{11}^E}D_2\right)\left(\frac{\partial w}{r\partial r}+\frac{\partial^2 w}{r^2\partial\theta^2}\right) + \frac{4}{3}h_1\overline{e}_{31}\varphi\right] + \frac{4\overline{e}_{31}}{h_1}[(h+h_1)^2-h^2]\varphi - \frac{\overline{e}_{31}^2(h+h_1)}{\overline{\Xi}_{33}}[(h+h_1)^2-h^2]\Delta w \tag{22}$$

$$M_{\theta\theta} = \int_{-h-h_1}^{h+h_1} z\sigma_{\theta\theta}\,dz = \int_{-h}^{h} z\sigma_{\theta\theta}^1\,dz + 2\int_{h}^{h+h_1} z\sigma_{\theta\theta}^2\,dz = -\left[\left(\mu D_1 + \frac{\overline{C}_{12}^E}{\overline{C}_{11}^E}D_2\right)\frac{\partial^2 w}{\partial r^2} + (D_1+D_2)\left(\frac{\partial w}{r\partial r}+\frac{\partial^2 w}{r^2\partial\theta^2}\right) + \frac{4}{3}h_1\overline{e}_{31}\varphi\right] + \frac{4\overline{e}_{31}}{h_1}[(h+h_1)^2-h^2]\varphi - \frac{\overline{e}_{31}^2(h+h_1)}{\overline{\Xi}_{33}}[(h+h_1)^2-h^2]\Delta w \tag{23}$$

$$M_{r\theta} = \int_{-h-h_1}^{h+h_1} z\tau_{r\theta}\,dz = \int_{-h}^{h} z\tau_{r\theta}^1\,dz + 2\int_{h}^{h+h_1} z\tau_{r\theta}^2\,dz = -\left[(1-\mu)D_1 + \left(1-\frac{\overline{C}_{12}^E}{\overline{C}_{11}^E}\right)D_2\right]\left(\frac{\partial^2 w}{r\partial r\partial\theta} - \frac{\partial w}{r^2\partial\theta}\right) \tag{24}$$

where $D_1=2Eh^3/3(1-\mu^2)$, $D_2=(2/3)h_1(3h^2+3hh_1+h_1^2)\bar{C}_{11}^E$.

The corresponding resultant shear forces are herein written as:

$$q_r = \frac{\partial M_{rr}}{\partial r} + \frac{\partial M_{r\theta}}{r\partial\theta} + \frac{M_{rr}-M_{\theta\theta}}{r} = -\left[(D_1+D_2)\frac{\partial}{\partial r}(\Delta w) + \frac{4}{3}h_1\overline{e}_{31}\frac{\partial \varphi}{\partial r}\right] + \frac{4\overline{e}_{31}}{h_1}[(h+h_1)^2-h^2]\frac{\partial \varphi}{\partial r} - \frac{\overline{e}_{31}^2(h+h_1)}{\overline{\Xi}_{33}}[(h+h_1)^2-h^2]\frac{\partial \Delta w}{\partial r} \tag{25}$$

$$q_\theta = \frac{\partial M_{r\theta}}{\partial r} + \frac{M_{\theta\theta}}{r\partial\theta} + \frac{2M_{r\theta}}{r} = -\frac{1}{r}\left[(D_1+D_2)\frac{\partial}{\partial\theta}(\Delta w) + \frac{4}{3}h_1\overline{e}_{31}\frac{\partial \varphi}{\partial\theta}\right] + \frac{4\overline{e}_{31}}{h_1}[(h+h_1)^2-h^2]\frac{\partial \varphi}{r\partial\theta} - \frac{\overline{e}_{31}^2(h+h_1)}{\overline{\Xi}_{33}}[(h+h_1)^2-h^2]\frac{\partial \Delta w}{r\partial\theta} \tag{26}$$

The governing equation of the Kirchhoff plate model is given by

$$\frac{\partial q_r}{\partial r}+\frac{\partial q_\theta}{r\partial\theta}+\frac{q_r}{r}-\left(\int_{-h}^{h}\rho_1\frac{\partial^2 u_z}{\partial t^2}\,dz+2\int_{h}^{h+h_1}\rho_2\frac{\partial^2 u_z}{\partial t^2}\,dz\right)=0. \tag{27}$$

Substitution of Eqs. (25) and (26) into Eq. (27) yields the governing equation for open circuit piezoelectric coupled plate

$$(D_1+D_2+D_4)\Delta\Delta w+\left(\frac{4}{3}h_1\bar{e}_{31}+D_3\right)\Delta\varphi+2(\rho_1 h+\rho_2 h_1)\frac{\partial^2 w}{\partial t^2}=0 \tag{28}$$

where $D_3=-4\bar{e}_{31}(2h+h_1)$, $D_4=\bar{e}_{31}(h+h_1)[(h+h_1)^2-h^2]/\overline{\Xi}_{33}$; ρ_1 and ρ_2 are material densities of the host plate and piezoelectric layers, respectively.

Substitution of Eqs. (18)–(20) and Eq. (21) into the Maxwell equation

$$\int_{h}^{h+h_1}\left[\frac{\partial(rD_r)}{r\partial r}+\frac{\partial D_\theta}{r\partial\theta}+\frac{\partial D_z}{\partial z}\right]dz=0 \tag{29}$$

leads to the differential equation for the electric field as follows:

$$B_1\Delta\varphi+B_2\Delta\Delta w+\frac{8\overline{\Xi}_{33}}{h_1}\varphi-\bar{e}_{31}h_1\Delta w=0 \tag{30}$$

where

$$B_1=\frac{4}{3}[(h+h_1)^3-h^3]\frac{\overline{\Xi}_{11}}{h_1^2}-2[(h+h_1)^2-h^2]\frac{\overline{\Xi}_{11}}{h_1}-\frac{2(2h+h_1)}{h_1^2}[(h+h_1)^2-h^2]\overline{\Xi}_{11}-\left[1+\frac{4(h+h_1/2)^2}{h_1}\right]h_1\overline{\Xi}_{11}+4h\overline{\Xi}_{11},$$

$$B_2=[(h+h_1)^2-h^2]\frac{\bar{e}_{31}(h+h_1)\overline{\Xi}_{11}}{2\overline{\Xi}_{33}}-\frac{\bar{e}_{31}h(h+h_1)\overline{\Xi}_{11}h_1}{\overline{\Xi}_{33}}$$

φ is solved by Eqs. (28) and (30),

$$\varphi=\frac{\bar{e}_{31}h_1^2}{8\overline{\Xi}_{33}}\Delta w-\frac{C_1h_1}{8\overline{\Xi}_{33}}\Delta\Delta w-\frac{C_2h_1}{8\overline{\Xi}_{33}}\frac{\partial^2 w}{\partial t^2} \tag{31}$$

where $C_1=(B_2-B_1)(D_1+D_2+D_4)/((4/3)h_1\bar{e}_{31}+D_3)$, $C_2=(-B_1)(2(\rho_1 h+\rho_2 h_1))/((4/3)h_1\bar{e}_{31}+D_3)$.

From Eqs. (31) and (28), we get the sixth-order differential equation about w

$$T_3\Delta\Delta\Delta w-T_2\Delta\Delta w+T_1\Delta\left(\frac{\partial^2 w}{\partial t^2}\right)-T_0\frac{\partial^2 w}{\partial t^2}=0 \tag{32}$$

where $T_0=2(\rho_1 h+\rho_2 h_1)$, $T_1=((4/3)h_1\bar{e}_{31}+D_3)(C_2h_1/8\overline{\Xi}_{33})$, $T_2=D_1+D_2+D_4+((4/3)h_1\bar{e}_{31}+D_3)(\bar{e}_{31}h_1^2/8\overline{\Xi}_{33})$, $T_3=((4/3)h_1\bar{e}_{31}+D_3)(C_1h_1/8\overline{\Xi}_{33})$.

The wave solution for $w(r,\theta,t)$ can be written as follows:

$$w(r,\ \theta,\ t)=\hat{w}(r)e^{i(p\theta-\omega t)}, \tag{33}$$

where $\hat{w}(r)$ is the amplitude of the z-direction displacement as a function of radial distance only; ω is the natural frequency of the coupled plate; and p is the wavenumber in θ direction.

The general solution of the sixth-order differential equation about $\hat{w}(r)$ can be obtained following a similar and standard process in Ref. [15], and the solution is directly given as below:

$$\hat{w}(r)=A_1Z_1(\mu_1 r)+A_2Z_2(\mu_2 r)+A_3Z_3(\mu_3 r) \tag{34}$$

where A_i is the unknown parameter, $\mu_1=\sqrt{|x_1|}$, $\mu_2=\sqrt{|x_2|}$, $\mu_3=\sqrt{|x_3|}$ and

$$Z_i(\mu_i r)=\begin{cases}J(\mu_i r), & x_i<0\\ I(\mu_i r), & x_i>0\end{cases}\quad(i=1,\ 2,\ 3)$$

$J(\circ)$ is the first type Bessel function and $I(\circ)$ is the modified first type Bessel function. As the structure is a solid disc, three solutions of Bessel function vanish. Thus, following Ref. [15], the roots of the cubic characteristic equation can be written as

$$x_1=2S\cos\frac{\psi}{3}+\frac{T_2}{3T_3} \tag{35}$$

$$x_2=2S\cos\frac{\psi+2\pi}{3}+\frac{T_2}{3T_3} \tag{36}$$

$$x_3=2S\cos\frac{\psi+4\pi}{3}+\frac{T_2}{3T_3} \tag{37}$$

where $S=(1/3T_3)\sqrt{T_2^2+3T_1T_3\omega^2}$, $\psi=\arccos(-c/2\sqrt{(-b/3)^3})$, $b=-(T_2^2/3T_3^2)-(T_1\omega^2/T_3)$, $c=-(2T_2^3/27T_3^3)-(T_1T_2\omega^2/3T_3^2)+(T_0\omega^2/T_3)$.

$\varphi(r,\theta,t)$ can thus be expressed as follows:

$$\varphi(r,\ \theta,\ t)=\hat{\varphi}(r)e^{i(p\theta-\omega t)} \tag{38}$$

where $\hat{\varphi}(r)$ is the spatial variation of the electric potential in the radial direction, which can be obtained directly by submitting Eqs. (33), (34) and (38) into Eq. (31)

$$\begin{aligned}\hat{\varphi}(r)=&\frac{1}{8}\left(\frac{\hat{w}^2C_2h_1}{\overline{\Xi}_{33}}-\frac{C_1h_1\mu_1^4}{\overline{\Xi}_{33}}+\frac{\overline{e}_{31}h_1^2\mu_1^2s_1}{\overline{\Xi}_{33}}\right)Z_1(\mu_1r)A_1+\frac{1}{8}\left(\frac{\hat{w}^2C_2h_1}{\overline{\Xi}_{33}}-\frac{C_1h_1\mu_2^4}{\overline{\Xi}_{33}}+\frac{\overline{e}_{31}h_1^2\mu_2^2s_2}{\overline{\Xi}_{33}}\right)Z_2(\mu_2r)A_2\\&+\frac{1}{8}\left(\frac{\hat{w}^2C_2h_1}{\overline{\Xi}_{33}}-\frac{C_1h_1\mu_3^4}{\overline{\Xi}_{33}}+\frac{\overline{e}_{31}h_1^2\mu_3^2s_3}{\overline{\Xi}_{33}}\right)Z_3(\mu_3r)A_3\end{aligned} \tag{39}$$

3. Solution for free vibration of open circuit piezoelectric coupled plate

The resonance frequencies and mode shapes for the coupled plate structure with two standard boundary conditions can be solved from an eigen value problem.

3.1. Clamped circular plate

Since the piezoelectric layer is assumed to abut vacuum, the electric displacement along r-direction, D_r, can be approximated to be zero at $r=r_0$. The boundary conditions of the clamped circular plate are expressed as

$$\hat{w}=0,\quad \hat{w}'=0,\quad \frac{\partial\phi}{\partial r}=0\quad(\text{at } r=r_0) \tag{40}$$

Substitution of Eqs. (34) and (39) into Eq. (40) yields the characteristic equation

$$\begin{vmatrix} m_{11} & m_{12} & m_{13}\\ m_{21} & m_{22} & m_{23}\\ m_{31} & m_{32} & m_{33}\end{vmatrix}=0, \tag{41}$$

where

$$\begin{aligned}m_{11}&=Z_1(\mu_1r_0)\\ m_{12}&=Z_2(\mu_2r_0)\\ m_{13}&=Z_3(\mu_3r_0)\\ m_{21}&=\alpha_1Z'_1(\mu_1r_0)\\ m_{22}&=\alpha_2Z'_2(\mu_2r_0)\\ m_{23}&=\alpha_3Z'_3(\mu_3r_0)\\ m_{31}&=\frac{1}{8\overline{\Xi}_{33}}(-C_1h_1\mu_1^4+\overline{e}_{31}h_1^2\mu_1^2s_1+\omega^2C_2h_1)\mu_1Z'_1(\mu_1r_0)\\ m_{32}&=\frac{1}{8\overline{\Xi}_{33}}(-C_1h_1\mu_2^4+\overline{e}_{31}h_1^2\mu_2^2s_2+\omega^2C_2h_1)\mu_2Z'_2(\mu_2r_0)\\ m_{33}&=\frac{1}{8\overline{\Xi}_{33}}(-C_1h_1\mu_3^4+\overline{e}_{31}h_1^2\mu_3^2s_3+\omega^2C_2h_1)\mu_3Z'_3(\mu_3r_0)\end{aligned} \tag{42}$$

From Eq. (41), resonant frequencies can be solved, and the corresponding mode shapes of the flexural displacement $\hat{w}$ and the electric potential $\hat{\varphi}$ are provided below:

$$\hat{w}=A_3\left[\frac{m_{13}m_{22}-m_{23}m_{12}}{m_{12}m_{21}-m_{11}m_{22}}Z_1(\mu_1r_0)+\frac{m_{11}m_{23}-m_{13}m_{21}}{m_{12}m_{21}-m_{11}m_{22}}Z_2(\mu_2r_0)+Z_3(\mu_3r_0)\right] \tag{43}$$

$$\begin{aligned}\hat{\varphi}=A_3\Bigg[&\frac{m_{13}m_{22}-m_{23}m_{12}}{m_{12}m_{21}-m_{11}m_{22}}\left(\frac{\hat{w}^2C_2h_1}{\overline{\Xi}_{33}}-\frac{C_1h_1\mu_1^4}{\overline{\Xi}_{33}}+\frac{\overline{e}_{31}h_1^2\mu_1^2s_1}{\overline{\Xi}_{33}}\right)Z_1(\mu_1r_0)\\&+\frac{m_{11}m_{23}-m_{13}m_{21}}{m_{12}m_{21}-m_{11}m_{22}}\left(\frac{\hat{w}^2C_2h_1}{\overline{\Xi}_{33}}-\frac{C_1h_1\mu_2^4}{\overline{\Xi}_{33}}+\frac{\overline{e}_{31}h_1^2\mu_2^2s_2}{\overline{\Xi}_{33}}\right)Z_2(\mu_1r_0)+Z_3(\mu_3r_0)\\&+\left(\frac{\hat{w}^2C_2h_1}{\overline{\Xi}_{33}}-\frac{C_1h_1\mu_3^4}{\overline{\Xi}_{33}}+\frac{\overline{e}_{31}h_1^2\mu_3^2s_3}{\overline{\Xi}_{33}}\right)\Bigg]\end{aligned} \tag{44}$$

It is assumed that steel and PZT4 are employed as the host structure and piezoelectric layer, respectively. The material properties and geometric sizes of piezoelectrically coupled plate are provided in Table 1. Fig. 2 provides the first four

Table 1
Material properties and geometric size of the piezoelectric coupled plate.

	Host structure (steel)	Piezoelectric layer (PZT4)
Young's module (N/m^2)	$E=200\times10^9$	$C_{11}^E=132\times10^9$ $C_{12}^E=71\times10^9$ $C_{33}^E=115\times10^9$ $C_{13}^E=73\times10^9$
Mass density (kg/m^3)	7.8×10^3	7.5×10^3
e_{31} (C/m^2)	–	-4.1
e_{33} (C/m^2)	–	14.1
Ξ_{11} (F/m)	–	7.124×10^{-9}
Ξ_{33} (F/m)	–	5.841×10^{-9}
r_0 (mm)	600	
h (mm)	10	
h_1 (mm)	2	

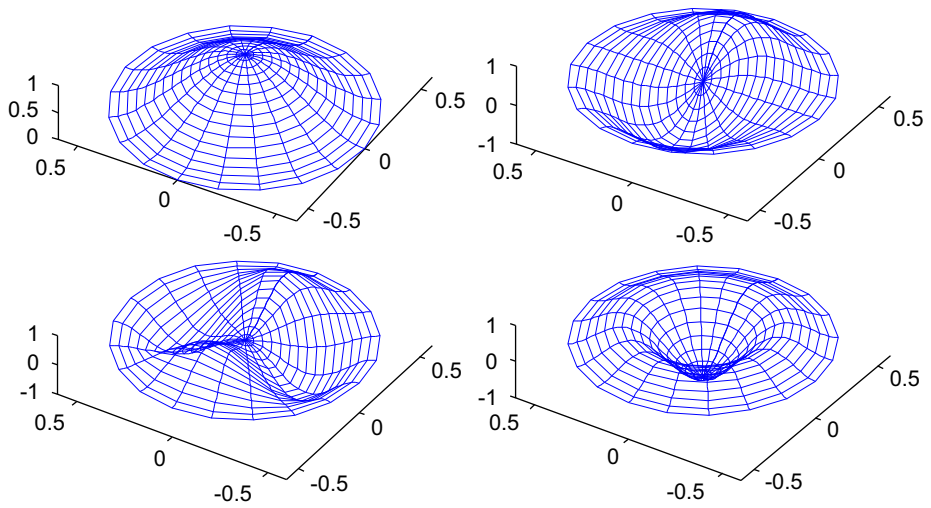

Fig. 2. First four mode shapes of the displacement of the open circuit piezoelectric coupled plate with clamped boundary condition.

vibration mode shapes of the displacement of the clamped open circuit piezoelectric coupled plate. Fig. 3 shows the electric potential distributions in thickness direction of the open and closed circuit piezoelectric layers.

3.2. Simply supported circular plate

For simply supported circular plate, boundary conditions are given by

$$\hat{w}=0,\quad \hat{M}_{rr}=0,\quad \frac{\partial\phi}{\partial r}=0\quad(\text{at } r=r_0) \tag{45}$$

The characteristic equation is expressed as

$$\begin{vmatrix} n_{11} & n_{12} & n_{13} \\ n_{21} & n_{22} & n_{23} \\ n_{31} & n_{32} & n_{33} \end{vmatrix}=0 \tag{46}$$

where

$$\begin{aligned} n_{11}&=Z_1(\mu_1 r_0)\\ n_{12}&=Z_2(\mu_2 r_0)\\ n_{13}&=Z_3(\mu_3 r_0)\\ n_{21}&=M_{11}+M_{12}+M_{13}\\ n_{22}&=M_{21}+M_{22}+M_{23} \end{aligned}$$

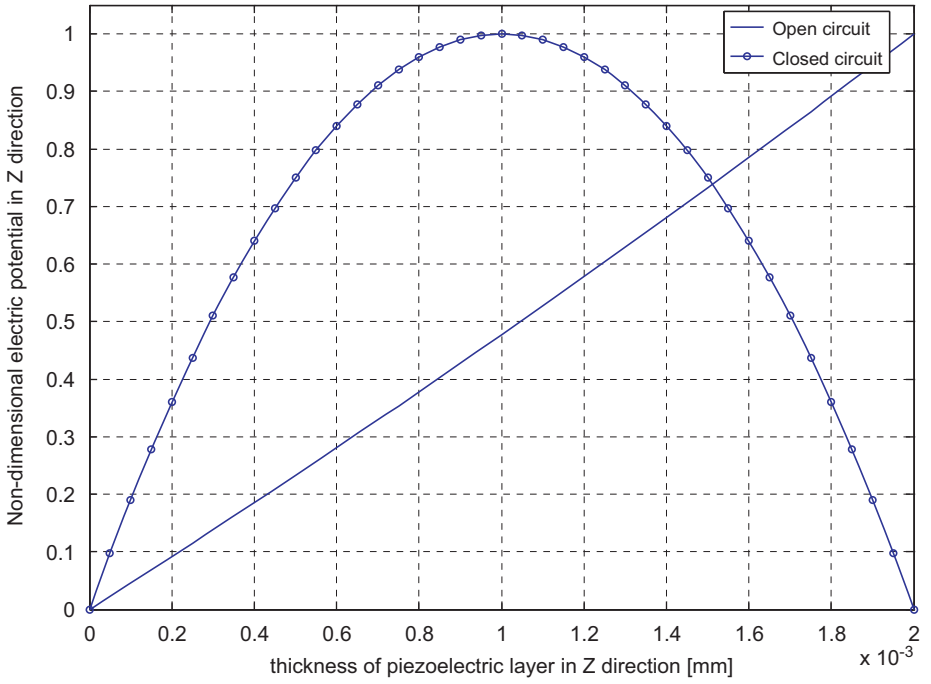

Fig. 3. The electric potential distributions in thickness direction of the open and closed circuit piezoelectric layers.

$$
\begin{aligned}
n_{23} &= M_{31}+M_{32}+M_{33}\\
n_{31} &= \frac{1}{8\overline{\Xi}_{33}}(-C_1h_1\mu_1^4+\overline{e}_{31}h_1^2\mu_1^2s_1+\omega^2C_2h_1)\mu_1Z'_1(\mu_1r_0)\\
n_{32} &= \frac{1}{8\overline{\Xi}_{33}}(-C_1h_1\mu_2^4+\overline{e}_{31}h_1^2\mu_2^2s_2+\omega^2C_2h_1)\mu_2Z'_2(\mu_2r_0)\\
n_{33} &= \frac{1}{8\overline{\Xi}_{33}}(-C_1h_1\mu_3^4+\overline{e}_{31}h_1^2\mu_3^2s_3+\omega^2C_2h_1)\mu_3Z'_3(\mu_3r_0).
\end{aligned}
\tag{47}
$$

M_{ii} is given by

$$
\begin{aligned}
M_{i1} = &\left[p^2\left(\frac{\mu D_1+\frac{C_{12}D_2}{C_{11}}}{D_1+D_2}-1\right)-s_i\mu_i^2r_0^2+\frac{1}{6}\frac{C_1h_1^2\overline{e}_{31}\mu_i^4r_0^2}{\overline{\Xi}_{33}(D_1+D_2)}+\frac{1}{6}\frac{\overline{e}_{31}^2h_1^3\mu_i^2s_ir_0^2}{\overline{\Xi}_{33}(D_1+D_2)}-\frac{1}{6}\frac{\overline{e}_{31}h_1^2\omega^2C_2}{\overline{\Xi}_{33}(D_1+D_2)}\right]Z_i(\mu_ir_0)\\
&+\left(1-\frac{\mu D_1+(C_{12}D_2/C_{11})}{D_1+D_2}\right)\mu_ir_0Z'_i(\mu_ir_0).
\end{aligned}
\tag{48}
$$

$$
M_{i2} = \frac{\overline{e}_{31}((h+h_1)^2-h^2)(-C_1h_1\mu_i^4-h_1^2\overline{e}_{31}\mu_i^2s_i+\omega^2C_2h_1)}{2\overline{\Xi}_{33}h_1(D_1+D_2)}r^2Z_i(\mu_ir_0)
\tag{49}
$$

$$
M_{i3} = -\frac{\overline{e}_{31}(h+h_1)((h+h_1)^2-h^2)s_i\mu_i^2}{\overline{\Xi}_{33}(D_1+D_2)}r_0^2Z_i(\mu_ir_0)\quad(i=1,\,2,\,3)
\tag{50}
$$

The deflection and electrical potential mode shapes are therefore provided to be

$$
\hat{w} = A_3\left[\frac{n_{13}n_{22}-n_{23}n_{12}}{n_{12}n_{21}-n_{11}n_{22}}Z_1(\mu_1r_0)+\frac{n_{11}n_{23}-n_{13}n_{21}}{n_{12}n_{21}-n_{11}n_{22}}Z_2(\mu_1r_0)+Z_3(\mu_3r_0)\right]
\tag{51}
$$

$$
\begin{aligned}
\hat{\varphi} = A_3&\left[\frac{n_{13}n_{22}-n_{23}n_{12}}{n_{12}n_{21}-n_{11}n_{22}}\left(\frac{\hat{w}^2C_2h_1}{\overline{\Xi}_{33}}-\frac{C_1h_1\mu_1^4}{\overline{\Xi}_{33}}+\frac{\overline{e}_{31}h_1^2\mu_1^2s_1}{\overline{\Xi}_{33}}\right)Z_1(\mu_1r_0)\right.\\
&+\frac{n_{11}n_{23}-n_{13}n_{21}}{n_{12}n_{21}-n_{11}n_{22}}\left(\frac{\hat{w}^2C_2h_1}{\overline{\Xi}_{33}}-\frac{C_1h_1\mu_2^4}{\overline{\Xi}_{33}}+\frac{\overline{e}_{31}h_1^2\mu_2^2s_2}{\overline{\Xi}_{33}}\right)Z_2(\mu_1r_0)+Z_3(\mu_3r_0)\\
&\left.+\left(\frac{\hat{w}^2C_2h_1}{\overline{\Xi}_{33}}-\frac{C_1h_1\mu_3^4}{\overline{\Xi}_{33}}+\frac{\overline{e}_{31}h_1^2\mu_3^2s_3}{\overline{\Xi}_{33}}\right)\right.
\end{aligned}
\tag{52}
$$

Fig. 4 shows the first four mode shapes of the displacement of the simply supported open circuit piezoelectric coupled plate.

4. Numerical simulations and discussions

In the following simulations, we adopt same material and geometry properties provided in Table 1.

Table 2 lists the first four resonance frequencies of both closed and open circuit piezoelectric coupled structures with a clamped boundary condition when the thickness ratio ($h_1/2h$) is 1/10. We can find that the resonant frequencies of the open and closed circuit piezoelectric coupled plates are increased by 6.73 percent and 3.77 percent, respectively, compared to the frequencies of the substrate steel. Such different increases in resonant frequencies of the two plates indicate that the effective stiffness of the open circuit piezoelectric coupled plate is larger than that of the closed circuit one, which coincides with the experimental results by Corr [17] and Chevallier [18]. In order to investigate the physical interpretation of the different increases, Table 3 lists the fundamental resonant frequencies of the open and closed circuit piezoelectric coupled plates with various piezoelectric layers at $h_1/2h$=1/10, 1/8, and 1/5, respectively, when the thickness of the host plate is 20 mm. The second column is calculated by removing the piezoelectric effect, or setting the piezoelectric

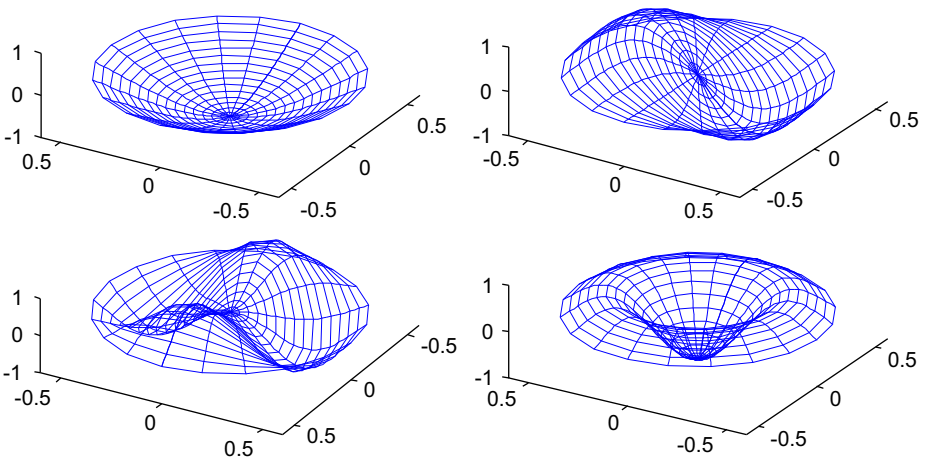

Fig. 4. First four mode shapes of the displacement of the open circuit piezoelectric coupled plate with simply supported boundary condition.

Table 2
The first four resonance frequencies of piezoelectric coupled plates with clamped boundary condition.

Mode number	Substrate plate	Piezoelectric coupled plate			
		Closed circuit [15]	Increments (%) closed circuit	Open circuit	Increments (%) open circuit
1	869.691	902.479	3.77	928.23	6.73
2	1809.87	1878.17	3.77	1931.76	6.73
3	2969.34	3081.08	3.76	3169.00	6.724
4	3385.71	3513.43	3.77	3613.69	6.73

Table 3
Effect of the circuit condition on the fundamental resonance frequencies of the piezoelectric coupled plate with clamped boundary condition at different thickness ratios.

Thickness ratio ($h_1/2h$)	Without piezoelectric effect	With piezoelectric effect			
		Closed circuit	Increment (%)	Open circuit	Increment (%)
1/10	902.40	902.479	0.0087	928.23	2.86
1/8	914.483	914.617	0.0147	946.45	3.50
1/5	957.87	958.356	0.0488	1007.5	5.19

Table 4
The first four resonance frequencies of piezoelectric coupled plates with simply supported boundary condition.

Mode number	Pure structure	Piezoelectric coupled			
		Closed circuit [15]	Increments (%) closed circuit	Open circuit	Increments (%) open circuit
1	420.33	435.6	3.63	448.067	6.74
2	1183.75	1227.5	3.70	1262.53	6.66
3	2181.51	2262.4	3.70	2327.03	6.67
4	2531.36	2625.2	3.75	2700.2	6.67

Table 5
Effect of the circuit condition on the fundamental resonance frequencies of the piezoelectric coupled plate with simply supported boundary condition at different thickness ratios.

Thickness ratio ($h_1/2h$)	Without electric contribution	With electric contribution			
		Closed circuit [15]	Increment (%)	Open circuit	Increment (%)
1/10	435.54	435.63	0.0206	448.067	2.88
1/8	441.30	441.42	0.027	456.91	3.54
1/5	462.04	462.34	0.065	486.73	5.34

coefficients to be null, to represent the only stiffening effect of the piezoelectric layer. Therefore, the percentages of the increase in the resonant frequency on columns 4 and 6 establish the piezoelectric effect clearly. From the table it is expectedly seen that the piezo-effect is obvious when the host plate is coupled with a thicker piezoelectric layer for both closed and open circuit conditions. In addition, the piezo-effect of closed circuit piezoelectric layer is found to be almost negligible, whereas piezo-effect of open circuit one plays a major role in increasing the frequency of the coupled plate. Such a phenomenon is attributed to the different electric potential distributions along thickness direction of the open and closed circuit of the piezoelectric layers. Fig. 3 shows the electric potential distributions in thickness direction of open and closed circuit piezoelectric layers. The electric potential of the closed circuit piezoelectric layer reaches maxima at the mid-plane of piezoelectric layer, then begins to decrease and returns to zero on the surface of piezoelectric layer. On the other hand, for the open circuit electric surface condition, the electric potential keeps growing to maxima towards the surface of piezoelectric layer. The distributions show that when a piezoelectric layer is shortly connected, the electric potential on both surfaces of the piezoelectric layer vanish, and hence the electric energy is released by the closed circuit electrode status, which would reduce the piezo-effect of the piezoelectric layer on the stiffness of the coupled plate. On the other hand, the electric potential of an open circuit piezoelectric layer cannot be released during any vibration of the coupled plate, and is continually converted to mechanical energy because of the piezo-effect. Such a process enlarges the increase of effective stiffness of the coupled structure. Therefore, higher piezo-effect could be observed from the open circuit piezoelectric layer.

The first four resonance frequencies of the piezoelectric coupled plate with a simply supported boundary condition are shown in Table 4. The thickness ratio of piezoelectirc layer to the host beam is 1/10, which is the same as the thickness ratio used in Table 2. Although the frequencies are found to be much lower than those of the plate with a clamped boundary condition, higher increases in resonance frequencies of the open circuit piezoelectric layer than those of the closed circuit piezoelectric plate is again observed. Such a result coincides with that of the clamped coupled plate. Table 5 lists the fundamental frequencies of the simply supported open and closed circuit piezoelectric coupled plates with various thickness piezoelectric layers when the thickness of the host beam is 20 mm. Similar observations on the differences of the piezo-effect between open and closed circuit piezoelectric layers are also obtained.

5. Conclusion

A mechanical model for the analysis of an open circuit piezoelectric coupled circular plate is developed. The solution for electric potential along thickness direction of piezoelectric layer is provided for the first time to strictly satisfy the open circuit electric boundary condition. Based on the developed electric potential solution and the Kirchhoff plate model and the Maxwell equation, the free vibration solution for the piezoelectric coupled plate is presented.

The numerical simulations show that the resonance frequencies of the open circuit piezoelectric coupled plate are higher than those of the closed circuit counterpart. Piezo-effects of the open and closed circuit piezoelectric layers are particularly investigated and found that the effect from the open circuit piezoelectric layer is much larger than that from the closed circuit one, which is almost negligible. Such a difference is owing to the different electric energy processes of the two piezoelectric layers during vibrations.

Acknowledgements

This research was undertaken, in part, thanks to funding from the Canada Research Chairs Program (CRC) and the National Science and Engineering Research Council (NSERC).

References

[1] A.A. Bent, N.W. Hagood, J.P. Rodgers, Anisotropic actuation with piezoelectric fiber composites, *Journal of Intelligent Material Systems and Structures* 6 (1995) 338–349.
[2] P.R. Heyliger, G. Ramirez, Free vibration of laminated circular piezoelectric plates and discs, *Journal of Sound and Vibration* 229 (1999) 935–956.
[3] D. Varelis, D.A. Saravanos, Coupled buckling and postbuckling analysis of active laminated piezoelectric composite plates, *International Journal of Solids and Structures* 41 (2004) 1519–1538.
[4] Q. Wang, K.M. Liew, Analysis of wave propagation in piezoelectric coupled cylinder affected by transverse shear and rotary inertia, *International Journal of Solids and Structures* 40 (2003) 6653–6667.
[5] S. Kapuria, P.C. Dumir, A. Ahmed, An efficient coupled layerwise theory for dynamic analysis of piezoelectric composite beams, *Journal of Sound and Vibration* 261 (2003) 927–944.
[6] W.H. Duan, S.T. Quek, Q. Wang, Free vibration analysis of piezoelectric coupled thin and thick annular plate, *Journal of Sound and Vibration* 281 (2005) 119–139.
[7] K.M. Liew, X.Q. He, T.Y. Ng, S. Kitipornchai, Active control of FGM shells subjected to a temperature gradient via piezoelectric sensor/actuator patches, *International Journal for Numerical Methods in Engineering* 55 (2002) 653–668.
[8] K.M. Liew, X.Q. He, S. Kitipornchai, Finite element method for the feedback control of FGM shells in the frequency domain via piezoelectric sensors and actuators, *Computer Methods in Applied Mechanics and Engineering* 193 (2004) 257–273.
[9] Z. Zhang, C. Feng, K.M. Liew, Three-dimensional vibration analysis of multilayered piezoelectric composite plates, *International Journal of Engineering Science* 44 (2006) 397–408.
[10] E.F. Crawley, J. Deluis, Use of piezoelectric actuators as elements of intelligent structures, *AIAA Journal* 25 (1987) 1373–1385.
[11] E.F. Crawley, E. Anderson, Detailed model of piezoelectric actuation of beams, in: Proceedings of the 30th AIAA/ASME/SAE Structures, Structural Dynamics, and Material Conference, Washington DC, April 1989, pp. 2000–2010.
[12] M.M. Leibowitz, J.R. Vinson, The use of Hamilton's principle in laminated piezoelectric and composite structures, *Adaptive Structures and Material Systems* (1993) AD-35.
[13] K.M. Liew, H.K. Lim, M.J. Tan, X.Q. He, Analysis of laminated composite beams and plates with piezoelectric patches using the element-free Galerkin method, *Computational Mechanics* 29 (2002) 486–497.
[14] Q. Wang, S.T. Quek, Flexural vibration analysis of sandwich beam coupled with piezoelectric actuator, *Smart Materials and Structures* 9 (2000) 103–109.
[15] Q. Wang, S.T. Quek, C.T. Sun, X. Liu, Analysis of piezoelectric coupled circular plate, *Smart Materials and Structures* 10 (2001) 229–239.
[16] C.L. Davis, G.A. Lesieutre, An actively tuned solid-state vibration absorber using capacitive shunting of piezoelectric stiffness, *Journal of Sound and Vibration* 232 (2000) 601–617.
[17] L.R. Corr, W.W. Clark, Comparison of low-frequency piezoelectric switching shunt techniques for structural damping, *Smart Materials and Structures* 11 (2002) 370–376.
[18] G. Chevallier, S. Ghorbel, A. Benjeddou, A benchmark for free vibration and effective coupling of thick piezoelectric smart structures, *Smart Materials and Structures* 17 (2008) 065007.
[19] X. Liu, Free vibration of thin and thick piezoelectric coupled circular plates, A Thesis for The Degree of Master of Engineering (2001) National University of Singapore.
[20] E. Pan, P. Heyliger, Free vibration of simply supported and multilayered magneto-electro-elastic plates, *Journal of Sound and Vibration* 252 (2002) 429–443.
[21] P. Heyliger, D.A. Saravanos, Exact free vibration analysis of laminated plates with embedded piezoelectric layers, *Journal of Acoustic Society of America* 98 (1995) 1547–1557.
[22] H. Ding, R. Xu, W. Chen, Exact solutions for free vibration of transversely isotropic piezoelectric circular plates, *Chinese Journal of Mechanics Press* 16 (2000) 141–147.
[23] H.F. Tiersten, *Linear Piezoelectric Plate Vibration*, Plenum Press, New York, 1969.